First-Principles Studies of Photoinduced Charge Transfer in Noncovalently Functionalized Carbon Nanotubes

ARTICLE *in* THE JOURNAL OF PHYSICAL CHEMISTRY C · JUNE 2013

Impact Factor: 4.77 · DOI: 10.1021/jp402600m · Source: arXiv

Iek-Heng Chu
University of California, San Diego

Dmitri Kilin
University of South Dakota

THE JOURNAL OF PHYSICAL CHEMISTRY C

Article

pubs.acs.org/JPCC

First-Principles Studies of Photoinduced Charge Transfer in Noncovalently Functionalized Carbon Nanotubes

Iek-Heng Chu,[†] Dmitri S. Kilin,[†,‡] and Hai-Ping Cheng*,[†]

[†]Department of Physics and Quantum Theory Project, University of Florida, Gainesville, Florida 32611, United States

[‡]Department of Chemistry, University of South Dakota, Vermillion, South Dakota 57069, United States

ABSTRACT: We have studied the energetics, electronic structure, optical excitation, and electron relaxation of dinitromethane molecules ($CH_2N_2O_4$) adsorbed on semiconducting carbon nanotubes (CNTs) of chiral index (n,0) (n = 7, 10, 13, 16, 19). Using first-principles density functional theory (DFT) with generalized gradient approximations and van der Waals corrections, we have calculated adsorption energies of dinitropentylpyrene, in which the dinitromethane is linked to the pyrene via an aliphatic chain, on a CNT. A 780 meV (18.0 kcal/mol) binding energy has been found, which explains why such aliphatic chain−pyrene units can be and have been used in experiments to bind functional molecules to CNTs. The calculated electronic structures show that the dinitromethane introduces a localized state inside the band gap of CNT systems of n = 10, 13, 16. and 19; such a state can trap an electron when the CNT is photoexcited. We have therefore investigated the dynamics of intraband relaxations using the reduced density matrix formalism in conjunction with DFT. For pristine CNTs, we have found that the calculated charge relaxation constants agree well with the experimental time scales. Upon adsorption, these constants are modified, but there is not a clear trend for the direction and magnitude of the change. Nevertheless, our calculations predict that electron relaxation in the conduction band is faster than hole relaxation in the valence band for CNTs with and without molecular adsorbates.

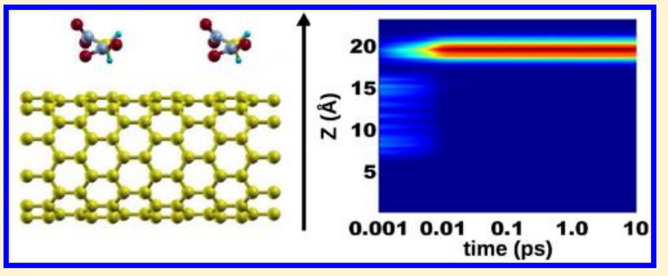

I. INTRODUCTION

Single-walled carbon nanotubes (CNTs) are formed by rolling monolayer graphene sheets in certain directions, characterized by the chiral vector $C_h = (n,m) \equiv n\mathbf{a}_1 + m\mathbf{a}_2$, where $\mathbf{a}_1$ and $\mathbf{a}_2$ are the lattice vectors for the graphene sheet.[1] This quasi-one-dimensional material is metallic when $n - m$ is divisible by 3; otherwise, it is semiconducting.

In the past two decades, CNTs have received intense attention[2−16] due to their unique tunable electronic properties, which lead to remarkable mechanical, thermal, and optical features. A variety of potential applications of CNTs have been studied by many experimental and theoretical groups in recent years, including the CNT-based nanosensing applications such as gas sensors,[4−9] which can detect gases such as O_2,[4] H_2,[5,7] or NO_2,[8,9] and photovoltaic solar cells,[10,11] in which the CNTs serve as electron acceptors and the conjugated polymers, for example P3OT, as electron donors. More recent experiments also used Si-CNT junctions to achieve solar cells with high efficiency.[12,13]

The interaction of CNTs with atoms or molecules is the key ingredient for utilizing CNTs as materials with desired functions and properties. There are two basic types of particle adsorption: chemisorption and physisorption. In chemisorption, the adsorbate, an atom or a molecule, is covalently or ionically bonded to the CNT. In physisorption, the van der Waals force becomes the dominant interaction between the adsorbate and the CNT, and the electronic structure of the CNTs only changes slightly; however, the dopants can introduce some localized states that are placed inside the band gap of semiconducting CNTs.[17] Depending on the relative energy of the localized state with respect to the valence band edge, n-type or p-type semiconducting CNT systems can be made. For problems related to photophysics and chemistry, these localized, midgap states open additional relaxation pathways to facilitate the electron transfer upon photoexcitations.[18] The rates for these processes, which measure how fast the electron in the CNT is transferred to the chemical species, are important quantities in the dynamics of such relaxation aided by lattice vibration. Therefore, an understanding of rates and hence the relaxation processes is of fundamental importance in device applications like photovoltaic solar cells and organic light-emitting diodes.

There are several treatments that can be used to study electron dynamics of interest. They are (i) complete active space configuration interaction (CAS-CI)[21] or time-dependent density functional theory (TDDFT),[22] which is then combined with methods such as Born−Oppenheimer molecular dynamics (MD),[23] Car−Parrinello MD,[24] force-field MD, etc.; (ii) the fewest-switches surface hopping in the time-dependent Kohn−Sham approach;[25−28] and (iii) the reduced density matrix

Received: March 14, 2013
Revised: August 4, 2013
Published: August 10, 2013

formalism[29] combined with DFT.[18,31−33] While CAS-CI or TDDFT based dynamics approaches can be applied to study excited states and photoinduced dynamics with high accuracy, their high computational costs limits their application to comparatively small-scale systems. The reduced density matrix formalism, which includes weak electron−phonon couplings, is an appropriate theoretical tool to study phonon-assisted processes, as it requires the least computation effort among the approaches mentioned above. Previously, Micha et al. have utilized this method to study the relaxation dynamics of Si surfaces with adsorbed Ag clusters,[18] and the results are consistent with experiments. Besides, Inerbaev et al. have applied this method to TiO_2 surfaces,[19] and Chen et al. have investigated the doped silicon quantum dots using this approach.[20]

In this paper, we report our investigations using first-principles methods to study the physisorption of dinitromethane $CH_2N_2O_4$ on semiconducting zigzag single-walled CNTs. This molecule contains a nitro group, which is known as a good electron acceptor. We have calculated the adsorption energies of dinitromethane or dinitropentylpyrene attached to various CNTs, electronic structures before and after molecular adsorption, and also photoexcitation and subsequent phonon-assisted intraband relaxation dynamics for dinitromethane physisorbed on CNTs. In particular, we have investigated such relaxation processes in the pristine CNTs since they have been studied in recent experiments.[34−38]

The work presented here is organized as follows. The model and the methods are introduced in section II; results are shown in section III, which contains three parts: (A) energetics and electronic structures of the systems; (B) *ab initio* molecular dynamics and nonadiabatic couplings, and (C) dynamics of the phonon-assisted relaxation upon initial photoexcitations; and conclusions are in section IV.

II. MODELS, METHODS, AND COMPUTATIONAL DETAILS

We have set up two types of theoretical models. The first one consists of a semiconducting $(n, 0)$ CNT and a dinitropentylpyrene, in which the dinitromethane $CH_2N_2O_4$ is linked, via an aliphatic chain, to the pyrene $C_{16}H_{10}$ (Figure 1A) that has been adsorbed on the CNT. The second one consists of the same $(n, 0)$ CNT but only a dinitromethane (Figure 1B) directly adsorbed on the CNT. Since the sizes of the adsorbate in both cases are different, the corresponding CNT supercells for adsorbates in the first and the second cases have been constructed to contain five and two CNT primitive cells, or 200 and 80 carbon atoms, respectively. Such a choice has guaranteed that the interactions between periodical images of the adsorbate are sufficiently weak. The two systems are shown in Figures 1C and 1D. The first model has been used to understand the enhanced binding between the functioning molecule and the CNT via the large contact area between the pyrene fragment and the CNT, as was found in experiments,[11,39,40] and the second model has served as a simplified model system for investigating electron dynamics of excitations.

The rest of this section details (A) the density functional theory (DFT) and approximations that have been used for the structural optimizations, energetics and the electronic structures and (B) the reduced density matrix formalism combined with the DFT that has been employed to study the dynamics of the phonon-assisted intraband relaxations in both the conduction band and the valence band.

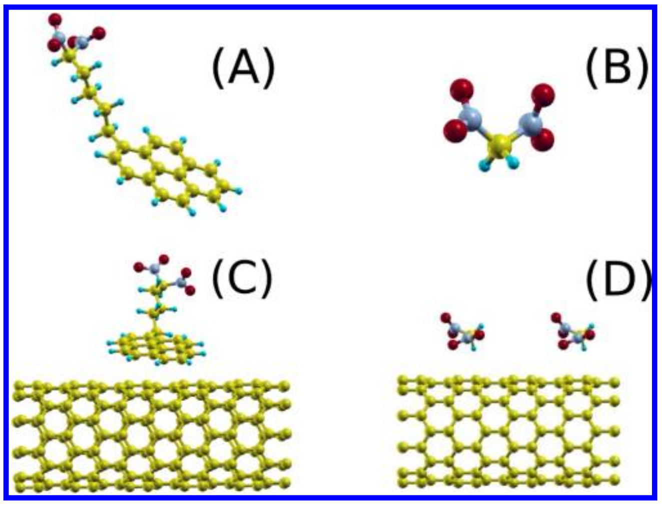

Figure 1. (A) The dinitropentylpyrene molecule, where the colors red, gray, blue, and yellow show oxygen, nitrogen, hydrogen, and carbon atoms, respectively. (B) The dinitromethane molecule. (C, D) CNT with a dinitropentylpyrene and with a dinitromethane, respectively. The figure is created using XCrysden.[41]

A. Density Functional Theory and Calculations.

1. Density Functional Theory. The foundations of DFT state that for an N-electron system all the ground-state physical properties can be determined once the ground-state charge density of the system is known. In this theory, the total energy of the system can be expressed as[33]

$$E_{\text{tot}} = \sum_{i=1}^{N} -\frac{\hbar^2}{2m}\int d\mathbf{r}\, \phi_i^*(\mathbf{r})\nabla^2\phi_i(\mathbf{r}) + \frac{1}{2}\int\int d\mathbf{r}\, d\mathbf{r}'\frac{\rho(\mathbf{r})\rho(\mathbf{r}')}{|\mathbf{r}-\mathbf{r}'|} + \int d\mathbf{r}\, V_{\text{ion}}(\mathbf{r})\rho(\mathbf{r}) + \int d\mathbf{r}\, \varepsilon_{\text{xc}}(\mathbf{r})\rho(\mathbf{r}) \tag{1}$$

where the charge density is $\rho(\mathbf{r}) = \sum_{a=1}^{N}|\phi_a(\mathbf{r})|^2$, $V_{\text{ion}}(\mathbf{r})$ is the potential from the ions, and $\varepsilon_{\text{xc}}(\mathbf{r})$ is the exchange-correlation functional of $\rho(\mathbf{r})$. There are many types of approximations to this functional, including (a) the local density approximation (LDA), in which ε_{xc} only depends on $\rho(\mathbf{r})$, (b) the generalized gradient approximation (GGA), where ε_{xc} depends on both $\rho(\mathbf{r})$ and $|\nabla\rho(\mathbf{r})|$, (c) GGA with inclusion of a semiempirical van der Waals (vdW) interaction, and (d) the vdW-DF functional, which includes the vdW interaction self-consistently.

Minimizing E_{tot} with respect to $\{\phi_i(\mathbf{r})\}$ along with the constraints $\int d\mathbf{r}\, \phi_i^*(\mathbf{r})\phi_j(\mathbf{r}) = \delta_{i,j}$, one arrives at the Kohn−Sham equation,[33] which reads

$$\left[-\frac{\hbar^2}{2m}\nabla^2 + V_{\text{eff}}(\mathbf{r})\right]\phi_i(\mathbf{r}) = \varepsilon_i\phi_i(\mathbf{r}) \tag{2}$$

$$V_{\text{eff}}(\mathbf{r}) = V_{\text{ion}}(\mathbf{r}) + \int d\mathbf{r}'\frac{\rho(\mathbf{r})}{|\mathbf{r}-\mathbf{r}'|} + V_{\text{xc}}(\mathbf{r}) \tag{3}$$

where $\{\phi_i(\mathbf{r})\}$ are known as the Kohn−Sham orbitals and $V_{\text{xc}}(\mathbf{r})$ is the exchange-correlation potential.

Since $V_{\text{eff}}(\mathbf{r})$ also depends on the total charge density, which is determined by the Kohn−Sham orbitals $\{\phi_i(\mathbf{r})\}$, the equation has to be solved self-consistently. The ground-state charge density $\rho(\mathbf{r})$ and the total energy can then be computed according to eq 1.

In general, when the system is in a nonequilibrium excited state, the charge density is composed as $\rho(\mathbf{r}) = \sum_{a,b}\rho_{ab}\phi_a^*(\mathbf{r})\phi_b(\mathbf{r})$ with ρ_{ab} the elements of the reduced density matrix in the basis of the Kohn−Sham orbitals. For a system in the ground state, the matrix elements become $\rho_{ab} = \delta_{a,b}f_a$ where $f_a = 1$ for $1 \le a \le N$ and zero otherwise. A brief introduction to the reduced density matrix formalism is given in the subsection B.

2. Energetics and Electronic Structures Calculations. The energetics, electronic structures, and structural optimizations have been performed using the Quantum Espresso (QE) package,[42] which utilizes the Rappe−Rabe−Kaxiras−Joannopoulos (RRKJ) ultrasoft pseudopotentials[43] and a plane-wave basis set. To understand how different exchange-correlation functionals affect the results, four different energy functionals have been examined: (a) the LDA exchange-correlation functional as parametrized by Perdew and Zunger;[44] (b) the Perdew−Burke−Ernzerhof (PBE) exchange-correlation functional[45] with the GGA method; (c) a semiempirical dispersion term, as proposed by Grimme[46] in conjunction with the PBE-GGA functional (we call it PBE + vdW); and (d) the vdW-density functional (vdW-DF) proposed by Dion et al.,[47,48] which includes the vdW interactions in the calculations self-consistently. The PBE-GGA without corrections does not include the van der Waals (vdW) binding,[49] which is important in our studies. The energy cutoff for the wave functions has been chosen as 40 Ry to ensure total energy convergence. The structures have been relaxed until the force on each atom is less than 0.01 eV/Å. Periodic boundary conditions have been applied along the tube axis, while a vacuum layer of 10 Å has been added in the other two directions to avoid nonphysical interactions between adjacent images.

When necessary, the electronic structure calculations have also been performed using the Vienna Ab-initio Simulation Package (VASP)[50,51] DFT code with the projector augmented wave (PAW) method.[52] In such calculations, the LDA exchange-correlation functionals or a new version of the vdW-DF which employs the optB86b exchange functionals[47,48,53] (optB86b vdW-DF) have been used.

To measure the interaction between the CNTs and adsorbates, we have calculated the binding energy E_b, which is defined as

$$E_b = E_{CNT} + E_m - E_{CNT+m} \tag{4}$$

where E_{CNT} and E_m are the total energies of the pristine CNT and the molecule, respectively. The binding is stable if E_b is positive.

B. Density Matrix Theory and Calculations. *1. Reduced Density Matrix Formalism.* In this subsection, we briefly describe the reduced density matrix formalism that has been used in our investigations. A thorough description of the theory can be found in refs 18, 29, and 31. For a closed system that consists of a subsystem of interest and a reservoir, the total Hamiltonian H can be written as a sum of the system part H_S, the reservoir part H_R, and the system−reservoir interaction H_{S-R}: $H = H_S + H_R + H_{S-R}$. The density operator for the whole system reads $\hat{\rho}_{tot}(t) = |\Phi(t)\rangle\langle\Phi(t)|$, where $|\Phi(t)\rangle$ is the pure state that represents the closed system. Since we are only interested in the system part, the reduced density operator (RDO) for the system part can be defined as $\hat{\rho}(t) = \mathrm{Tr}_R\{\hat{\rho}_{tot}(t)\} = \sum_R\langle\phi_R(t)|\hat{\rho}_{tot}(t)|\phi_R(t)\rangle$; the trace of the density operator in the reservoir space yields the RDO for the system part. In the energy representation where H_S is diagonal and its eigenstates $\{|\phi_n\rangle\}$ form an orthonormal basis set, the Markovian equation of motion for the RDO can be expressed as

$$\frac{d\rho_{ab}(t)}{dt} = -\frac{i}{\hbar}\{[\hat{H}_S, \hat{\rho}(t)]\}_{ab} + \left(\frac{\partial\rho_{ab}}{\partial t}\right)_{diss} \tag{5}$$

$$\left(\frac{\partial\rho_{ab}}{\partial t}\right)_{diss} = -\sum_{cd} R_{ab,cd}\rho_{cd}(t) \tag{6}$$

where $\rho_{ab}(t) \equiv \langle\phi_a|\hat{\rho}(t)|\phi_b\rangle$ and $R_{ab,cd}$ are the elements of the reduced density matrix and of the Redfield tensor, respectively. The Redfield tensor R describes the interaction between the system and the reservoir and the elements of which can be expressed in terms of the Fourier components of the reservoir time-correlation function.[29,30] The second term on the right-hand side of eq 5, or eq 6, captures the irreversible dynamics of the energy dissipation from the system to the reservoir. It is convenient to work for the Redfield tensor in the interaction picture[29]

$$\left(\frac{\partial\rho_{ab}^{(I)}}{\partial t}\right)_{diss} = -\sum_{cd} e^{i(\omega_{ab}-\omega_{cd})\Delta t}R_{ab,cd}\rho_{cd}^{(I)}(t) \tag{7}$$

with $\rho_{ab}^{(I)} = \exp(i\omega_{ab}\Delta t)\rho_{ab}^{(t)}$. Here, Δt is the time step, which needs to be larger than the time scale given by the reservoir time correlation function so that the Markov approximation holds. The term $\hbar\omega_{ij} = \varepsilon_i - \varepsilon_j$ is the electronic transition energy. Since the phase factors oscillate rapidly, only terms with $\omega_{ab} - \omega_{cd} = 0$ survive after the long time average using a time $\tau \gg \Delta t$. This is known as the secular approximation,[29] which gives rise to two different cases: (i) $a = b$, $c = d$; (ii) $a \neq b$, $a = c$, $b = d$. Therefore, eq 7 can be separated into two sets of equations that read[29]

(i) population transfer:

$$\left(\frac{\partial\rho_{aa}}{\partial t}\right)_{diss} = -\sum_{c} R_{aa,cc}\rho_{cc}(t) \tag{8}$$

$$R_{aa,cc} = \delta_{ac}\sum_{e} k_{ae} - k_{ca} \tag{9}$$

(ii) coherence dephasing:

$$\left(\frac{\partial\rho_{ab}}{\partial t}\right)_{diss} = -R_{ab,ab}\rho_{ab}(t) \tag{10}$$

$$R_{ab,ab} = \sum_{c}\frac{1}{2}(k_{ac} + k_{bc}) + \gamma_0 \tag{11}$$

where k_{ab} is the transition rate from $|\phi_a\rangle$ to $|\phi_b\rangle$ and γ_0 is the pure dephasing constant.[54] When the electrons comprise the system while the ions are considered as the reservoir,[55] the rate coefficients k_{ab} are[18,31]

$$k_{ab} = \frac{1}{\hbar^2}|V_{ab}|^2 J(\omega_{ab})[n(\omega_{ab}, T) + 1] \tag{12}$$

where $V_{ab} = -i\hbar\langle\phi_a|\partial/\partial t|\phi_b\rangle$ is called the nonadiabatic coupling between $|\phi_a\rangle$ and $|\phi_b\rangle$, which depends on the ionic trajectories $\{\mathbf{R}(t)\}$. The factor $J(\omega) = \sum_j\delta(\omega_j - \omega)$ is the vibrational density of states, and $n(\omega,T) = [\exp(\hbar\omega/k_BT) - 1]^{-1}$ is the phonon occupation number for a mode with angular frequency ω at temperature T. Note that three parameters need to be determined beforehand: (i) the vibrational density of

Table 1. Binding Energies E_b Defined in Eq 4 and the Optimized Distances d between the (10,0) CNT and the Adsorbate Dinitropentylpyrene or Dinitromethane, Using Four Different Exchange-Correlation Functionals[a]

system	V_{xc}	E_b (meV)	E_b (kcal/mol)	d (Å)
adsorbate dinitropentylpyrene	PBE-GGA	6.1	0.1	4.03
	PBE + vdW	780	18.0	3.23
	LDA	380 (399)	8.8 (9.2)	3.25 (3.14)
	vdW-DF	880 (1040)	20.3 (24.0)	3.25 (3.13)
adsorbate dinitromethane	PBE-GGA	47.8	1.1	3.96
	PBE + vdW	270	6.2	3.50
	LDA	180 (216)	4.2 (5.0)	3.52 (3.36)
	vdW-DF	377 (354)	8.7 (8.2)	3.67 (3.53)

[a]The values in the parentheses are computed using VASP.

states J, (ii) the phonon occupation n, and (iii) nonadiabatic couplings V_{ab}.

2. Dynamics of the Intraband Relaxation. We have used eq 8 along with eqs 9 and 12 in the previous subsection to study the dynamics of the electronic relaxation in both the conduction band and the valence band upon initial photoexcitations. The transition dipole moments and oscillator strengths of the various electronic excitations have been calculated and used to determine the most optically active electronic state.[56] The transition dipole moment between states a and b, $\mathbf{D}_{ab}$, is defined as $\mathbf{D}_{ab} \equiv \langle \phi_a | r | \phi_b \rangle$, and the oscillator strength is expressed as

$$f_{ab} = \frac{2m\omega_{ab} |\mathbf{D}_{ab}|^2}{\hbar} \tag{13}$$

The nonadiabatic couplings in eq 12, which describe the electron−phonon interactions, have been computed based on an *ab initio* molecular dynamics. The system is initially heated up to 300 K by repeated velocity rescaling, and then the dynamics has been performed in the microcanonical ensemble, which yields the ionic trajectories. At any two consecutive time steps t and $t + \Delta t$, we have recalculated the Kohn−Sham orbitals $|\phi_a(t)\rangle$, $|\phi_b(t)\rangle$, $|\phi_a(t + \Delta t)\rangle$, and $|\phi_b(t + \Delta t)\rangle$, and the couplings are computed using finite difference increment. The final nonadiabatic coupling square $|V_{ab}|^2$ is approximated as the average over all those values. The coupling parameter converges if the time window for averaging is large enough. Numerical values of the coupling and the convergence of the averaging procedure are reported in the Results section.

After solving eq 8, we have studied the population distribution in the energy and time domain as well as the charge density distribution in the conduction band as functions of time t and height z, which is defined as distance perpendicular to the tube axis from the CNT to the C atom in the adsorbate. The distributions are defined in the following: A nonequilibrium population distribution in the energy and time domain reads[18] $n^{(a,b)}(\varepsilon,t) = \sum_i \rho_{ii}^{(a,b)}(t)\delta(\varepsilon_i - \varepsilon)$, where (a, b) denotes the initial photoexcitation from state a to state b. The change of the population with respect to the equilibrium distribution is then expressed as

$$\Delta n^{(a,b)}(\varepsilon, t) = n^{(a,b)}(\varepsilon, t) - n^{\mathrm{eq}}(\varepsilon) \tag{14}$$

This equation describes a population gain when $\Delta n > 0$ and a loss when $\Delta n < 0$ at energy ε, which corresponds to the electrons and holes.

The charge density distribution in the conduction band as functions of z and t is defined as[18]

$$P_{CB}^{(a,b)}(z, t) = \sum_{i,j \in CB} \rho_{i,j}^{(a,b)}(t) \int \mathrm{d}x\, \mathrm{d}y\, \phi_i^*(\mathbf{r})\phi_j(\mathbf{r}) \tag{15}$$

where $\phi_i(\mathbf{r})$ is the ith Kohn−Sham orbital, and the indices i and j belong to the conduction band. This distribution reflects the time evolution of the charge transfer along the z direction from the CNT into the adsorbate.

Finally, the time evolution of the population of the lowest unoccupied molecular orbital (LUMO) as well as the highest occupied molecular orbital (HOMO) can be fitted to the equation

$$P_{e(h)}(t) = 1 - \exp\left(\frac{-t}{\tau^{e(h)}}\right) \tag{16}$$

where e and h refer to the electron in the conduction band and the hole in the valence band, respectively. The constant $\tau^{e(h)}$ represents the average relaxation time for the electron (hole) and thus the dynamics of the electronic relaxation.

III. RESULTS

A. Energetics and Electronic Structure. We have prepared two groups of systems that consist of zigzag semiconducting CNTs with chiral indices $(n,0)$ (n = 7, 10, 13, 16, 19) adsorbed with either (1) a dinitropentylpyrene or (2) a dinitromethane, as shown in Figure 1. The $(n,0)$ CNTs with $n \geq 10$ have radius large enough such that they be easily made in experiment. To obtain ground-state electronic structures and binding energies, we have first optimized structures of these model systems. For physisorption, it is known that different exchange-correlation functionals may lead to different binding distance between the CNT and the adsorbate[49] and also to different binding energy. To test this, we have performed calculations using the four different functionals for a (10,0) CNT with the dinitropentylpyrene that contains a pyrene fragment. The resulting binding energies computed according to eq 4, and the CNT−molecule distances are shown in Table 1. The binding energy given by the PBE-GGA is only 6.1 meV (0.1 kcal/mol), and the equilibrium distance is 4.03 Å. When semiempirical vdW interactions are taken into account[46] along with the PBE exchange-correlation functionals (PBE + vdW), the binding energy becomes 780 meV (18.0 kcal/mol), and the corresponding distance is 3.23 Å. When using LDA, the binding energy and the distance are 380 meV (8.8 kcal/mol) and 3.25 Å, respectively. According to our results, the vdW interaction is important in our system; it is the main interaction between the pyrene fragment in the adsorbate and the CNT. This is consistent with Woods et al.'s[49] results for the interactions between benzene molecules and CNTs. It is

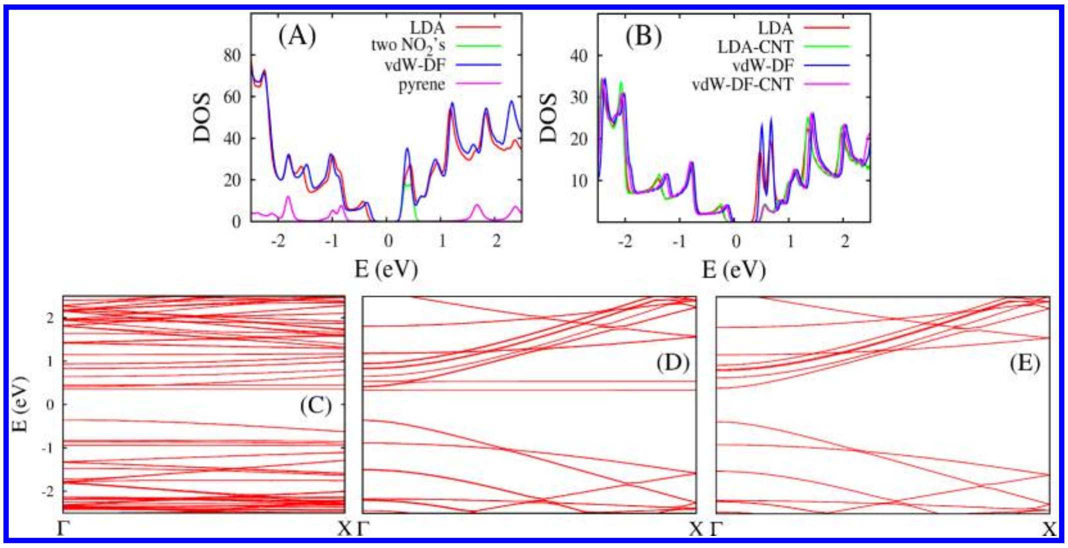

Figure 2. DOS and band structures in two model systems obtained from LDA and optB86b vdw-DF calculations. (A, C) The DOS and band structure for (10,0) CNT with dinitropentylpyrene. In (A), the projected DOS of the two nitrogen dioxides as well as that of the pyrene fragment are also shown. (B, D) The DOS and band structure for dinitromethane physisorbed on (10,0) CNT. (C, D) The flat bands near the band gap come from the adsorbates. (E) The band structure for the pristine (10,0) CNT for comparison. The Fermi energy is set to be zero.

clear that the LDA exchange-correlation functional gives results similar to those for the PBE + vdW. Finally, we have applied to our system the vdW-DF functional,[47,48] which includes the vdW interactions in the exchange-correlation functional and thus in the self-consistent procedure. The optimized atomic structure and the CNT−molecule distance are found to be similar to those obtained from the PBE + vdW or LDA calculations.

In the situation where a single dinitromethane molecule has been physisorbed on the (10,0) CNT, we have obtained results that lead to the same trend. Without the pyrene fragment, the binding energy now becomes much smaller in cases when LDA, PBE + vdW, and vdW-DF have been used; for example, the binding energy in the PBE + vdW case is reduced to only 270 meV (6.2 kcal/mol), a factor of 3 smaller than the value computed in the presence of the pyrene fragment. The optimized distance d, defined as the shortest distance between the CNT and the C atom in the dinitromethane molecule, is now 3.20 Å. This suggests that the pyrene fragment enhances the binding between the adsorbate and the CNT and that pyrene is a good choice for anchoring functional groups on CNTs. Note that the binding energy is much higher than the thermal energy at 300 K, which is about 26 meV (0.6 kcal/mol). Therefore, we expect that the molecule stays physisorbed around room temperature.

We have also repeated our calculations using VASP. In these calculations, the LDA exchange-correlation functional and the optB86b vdW-DF with the PAW method have been employed. The binding energies as well as the CNT−adsorbate distances are given in Table 1. We have found that the computed distances in all the cases decrease by about 3−4% compared with those from QE calculations.

For each adsorbate depicted in Figure 1A or 1B, we have computed the band structures and the density of states (DOS). Figure 2 shows the DOS as well as the band structure in each situation from the LDA calculations. When the pyrene anchoring fragment is present in the adsorbate, the peak observed immediately above the band gap observed in the DOS (Figure 2A) is attributed to the two NO_2 units in the dinitromethane. Without the pyrene fragment, the dinitromethane is closer to the CNT, which leads to an increase in the interaction between the CNT states and the states of the two NO_2s, and thus the peak splits into two (Figure 2B). The corresponding band structures for both situations are shown in Figures 2C and 2D. Near the conduction band edge, there are two molecular bands that have vanishing dispersion and do not depend on the k-vector. One of them is located inside the band gap while the other one is above it. Here, the important point is that the pyrene fragment in the dinitropentylpyrene does not provide states near the band gap, as shown in Figure 2A. Instead, it only acts to anchor the dinitromethane to the (10,0) CNT. The electronic structures obtained from PBE + vdW functionals are similar to the LDA results, and they are not shown here. The DOS plots from the optB86b vdW-DF using VASP are depicted in Figures 2A and 2B for both situations. In the presence of the pyrene fragment, the DOS from the vdW-DF calculations are very similar to the LDA results except that the band gap is now reduced by about 0.15 eV. The same conclusion can be drawn when the dinitromethane molecule is directly physisorbed on the (10, 0) CNT, but the reduction of the band gap is now about 0.2 eV. On the basis of the calculated electronic structures, we expect that the dynamics of the intraband electronic relaxation using the adsorbate dinitropentylpyrene or dinitromethane should be very similar. For computational efficiency, the small-size system that contains the single dinitromethane has been chosen for investigating the dynamics of the phonon-assisted intraband relaxation upon initial photoexcitation. Also, the following calculations of the dynamics of the intraband relaxations have been performed using the optB86b vdW-DF.

B. Molecular Dynamics and Nonadiabatic Couplings. We have performed the *ab initio* molecular dynamics for the nonadiabatic couplings in the (10,0) CNT with and without the adsorbate. The time step used in all these calculations is 0.5 fs. As a first step, we thermalize the systems up to 300 K by repeated velocity rescaling. To guarantee that the corresponding temperature increase is small enough that the thermalization is stable, we have gradually heated systems up to 300 K:

starting from the ground-state atomic structures, each time we heat systems to 100 K higher than the previous time, with 600 steps between two temperatures.

To confirm that systems are thermalized at 300 K and to calculate the nonadiabatic couplings, we then perform 600-step molecular dynamics in the microcanonical ensemble for both systems. The temperature as a function of number of time steps is plotted for both the pristine and functionalized (10,0) CNT in Figure 3. As shown in the figure, the temperature fluctuates within 20% around 300 K in both systems.

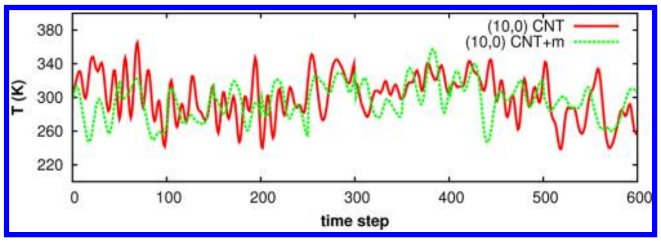

Figure 3. Temperature as a function of the number of time steps in *ab initio* molecular dynamics within the microcanonical ensemble. The red solid line and the green dashed line correspond to the one in (10,0) CNT without and with the molecule, respectively.

Next, at any two consecutive time steps, the nonadiabatic couplings between any two states a and b in the conduction band and/or in the valence band are computed, and the final coupling squares $|V_{ab}|^2$ are approximated as the average over all those values. As an example, Figure 4A shows the convergence

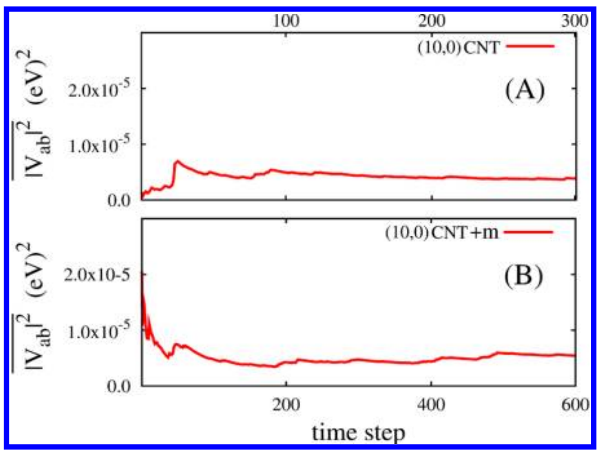

Figure 4. Average of nonadiabatic coupling square $\overline{|V_{ab}|^2}$ as a function of number of time steps in (A) pristine (10,0) CNT and (B) (10,0) CNT with the molecule. Here, a refers to HOMO, and b refers to the HOMO−3 and HOMO−2 for the pristine (10,0) CNT and the (10,0) CNT plus molecule, respectively.

of the coupling square of a pristine (10,0) CNT for a = HOMO and b = HOMO−3. The converged value is 3.8×10^{-6} (eV)^2. For comparison, the coupling square in the (10,0) CNT−adsorbate system is given in Figure 4B. The converged value, 5.4×10^{-6} (eV)^2, is larger than in the pristine (10,0) CNT.

C. Dynamics of the Phonon-Assisted Relaxation. If the system is optically excited at $t < 0$ by steady light with frequency $\Omega = (\varepsilon_b - \varepsilon a)/\hbar$, an electron can be excited from state a in the valence band to state b in the conduction band. For $t \geq 0$, the light is turned off and the electron begins the relaxation toward the LUMO and the hole toward the HOMO.

In the pristine (10,0) CNT, the electron at HOMO−2 is initially photoexcited to LUMO + 3, which is the most optically active state according to the oscillator strength values. The intraband relaxation dynamics is then investigated in the pristine (10,0) CNT. Figure 5B depicts the change of the nonequilibrium population distribution in the energy and time domains. The electron relaxation in the conduction band takes place rapidly. The LUMO starts to gain the electron population at the time of 1 fs and arrives its maximum at about t = 10 fs. However, the hole population is not completely transferred to the HOMO until about t = 1 ps, which is much slower than the electron population transfer. Figure 5D describes the time evolution of the charge density distribution in the conduction band along the z direction. The change of such distribution completes at about t = 10 fs.

The average electron and hole relaxation time constants for pristine (10,0) CNT obtained using eq 16 are given in Table 2 for initial photoexcitations selected according to oscillator strength values. The relaxation time constant for the electron is about 35 times smaller than for the hole. We have also repeated our calculations in the pristine (7,0), (13,0), (16,0), and (19,0) CNTs, with results also shown in Table 2. There are a few things worth pointing out: First, the relaxation times for the electrons are smaller than those of the holes in all the CNTs; an electron in the conduction band relaxes more rapidly than the hole in the valence band, which agrees with Habenicht et al.'s results[27] of intraband relaxations for (7,0) CNT. In their paper, they claim that the hole in the valence band interacts more strongly with the radial-breathing phonon mode (RBPM) than with the G-type longitudinal optical phonon mode (LOPM) in the CNT, while the electron in the conduction band mainly interacts with the latter mode. The transition rate between two states depends on the nonadiabatic coupling as well as the number of phonons at the state energy difference. In our studies, the corresponding phonon energy for the LOPM is about 180 meV while it is less than 80 meV for the RBPM, in all the pristine CNT systems. We have found that the energy differences for adjacent, nondegenerate states $\varepsilon_{i+1} - \varepsilon_i$ are closer to the LOPM phonon energy, which suggests that the LOPM plays an important role in the phonon-assisted relaxations. In the (10,0), (13,0), and (16,0) CNTs, we have also found that the nonadiabatic couplings for adjacent conduction band states are about an order of magnitude larger than those for valence band states. In (7,0) and (19,0) CNT, the couplings for conduction band states are about 2 times larger than those for valence band states. Therefore, the electron couples with the phonon stronger than the hole does, which results in a faster electron relaxation dynamics.

Second, the hole relaxation time constant in the pristine (7,0) CNT is 595 fs, while the electron relaxation time constant is only 121 fs. These are comparable with the time scales computed in ref 27. Third, the calculated hole relaxation time constants vary between 65 to 595 fs. The relaxation time constants of the electron, on the other hand, change from 1 fs to about 121 fs. Overall, the relaxation time constants calculated in the pristine CNTs agree well with the experimental time scales,[34−38] which vary from less than 100 fs to about 1 ps due to the complicated local environments in the samples.

With the single dinitromethane physisorbed on the $(n,0)$ CNTs, where n = 10, 13, 16, and 19, we have also calculated the electron and hole time constants upon initial photoexcitations as in the pristine $(n,0)$ CNT cases. Once again, the corresponding oscillator strength value in each case is large,

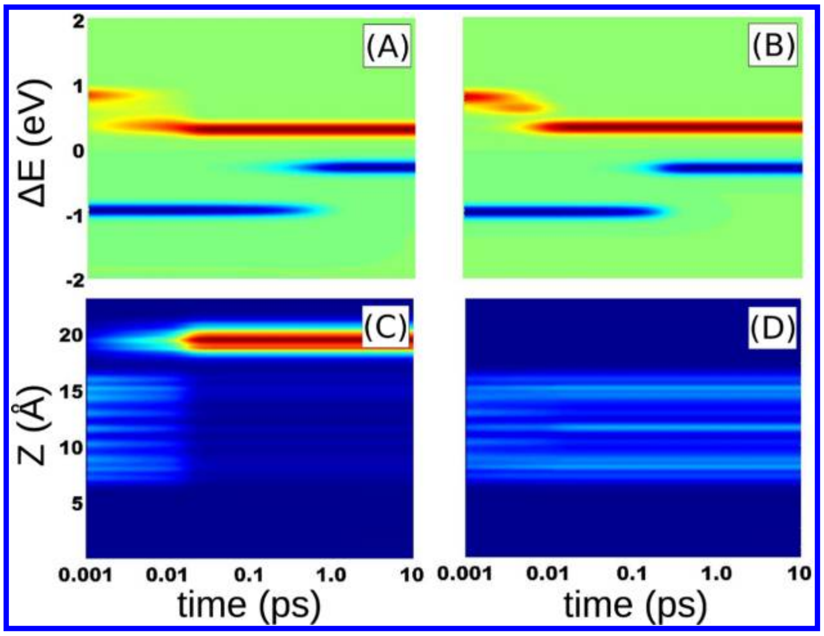

Figure 5. (A, B) Isocontours of the change of the population distribution $\Delta n(\Delta\varepsilon,t)$ in eq 14 from the dynamics of similar initial photoexcitations for the (10,0) CNT (A) with and (B) without dinitromethane, in the energy-time domain. The red, blue and green areas represent gain, loss and no change of population relative to the equilibrium distribution, respectively. The initial photoexcitations are from HOMO−2 to LUMO + 5 in (A) and from HOMO−2 to LUMO + 3 in (B). (C, D) Spatial distributions of the charge density in conduction band $P_{CB}(z,t)$ in eq 15 for the (10,0) CNT (C) with and (D) without dinitromethane. Color from blue to red indicates the charge density values from 0 to 1, and the direction Z points from the (10,0) CNT to the adsorbate.

Table 2. Electron (Hole) Relaxation Time Constants $\tau^{e(h)}$ Defined in Eq 16 for Different Pristine $(n,0)$ CNTs, with Given Initial and Final Electron−Hole Pair Excitation Transition Energies ΔE_i and ΔE_f, respectively; f_{if} Defined in Eq 13 Is the Oscillator Strength Corresponding to the Initial Photoexcitation

n	transition	f_{if}	ΔE_i (eV)	ΔE_f (eV)	τ^e (fs)	τ^h (fs)
7	HO−5 → LU+6	0.25	3.71	0.70	121	595
10	HO −2 → LU+3	0.82	1.76	0.65	12	416
13	HO −6 → LU+2	0.99	2.69	0.53	1	65
16	HO−12 → LU+3	1.50	2.95	0.45	4	199
19	HO−13 → LU+2	1.73	2.67	0.37	10	81

indicating that those excitations are optically active. The results are given in Table 3. Upon adsorption, our studies of electronic structures show that there is a gap state provided by the adsorbate in each case, as shown in Figure 6, and the electron relaxation time constants are much smaller than the hole relaxation time constants. Again, this is due to larger nonadiabatic couplings in the conduction band than in the valence band. The relaxation time constants as functions of the chiral index n, which in this situation is proportional to the tube radius, are visualized in Figure 7. It is clear that the relaxation time constants depend on the tube radius. Compared with the

Table 3. Electron (Hole) Relaxation Time Constants $\tau^{e(h)}$ for Different $(n,0)$ CNTs upon Adsorption of a Dinitromethane Molecule, with Similar Initial Photoexcitations as Those Shown in Table 2 for Pure CNTs

n	transition	f_{if}	ΔE_i (eV)	ΔE_f (eV)	τ^e (fs)	τ^h (fs)
10	HO−2 → LU+5	0.53	1.76	0.58	6	622
13	HO−7 → LU+4	1.19	2.69	0.50	2	123
16	HO−12 → LU+5	1.33	2.94	0.42	6	107
19	HO−13 → LU+4	1.84	2.68	0.37	11	169

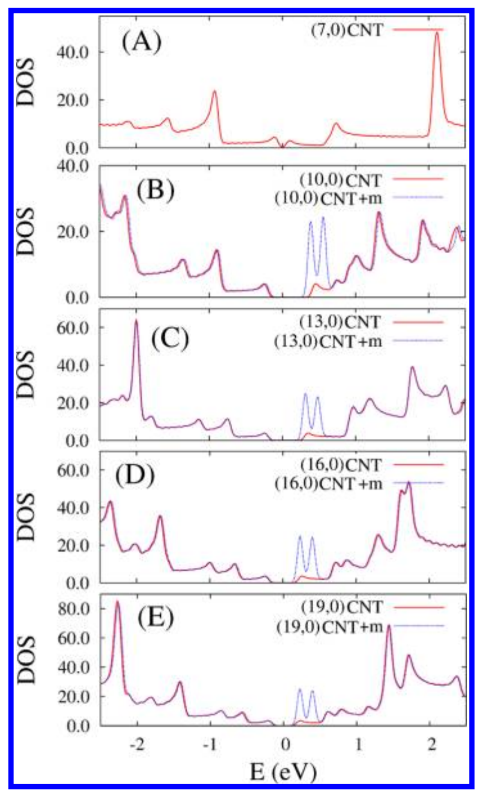

Figure 6. DOS for different pristine $(n,0)$ CNTs with (A) $n = 7$, (B) $n = 10$, (C) $n = 13$, (D) $n = 16$, and (E) $n = 19$. The DOS for $(n,0)$ CNTs physisorbed with the dinitromethane are also given in panels B−E.

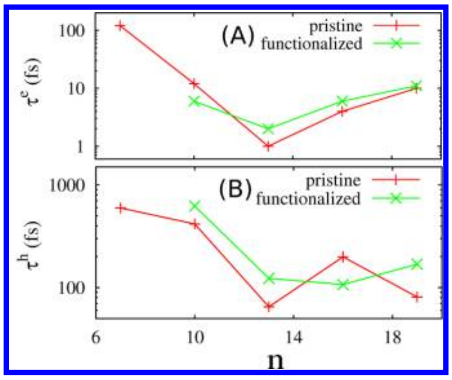

Figure 7. (A) Electron relaxation time constant, τ^e, and (B) hole relaxation time constant, τ^h, versus the chiral index, n, for the pristine (n,0) CNTs and for (n,0) CNT functionalized by dinitromethane.

results of the intraband relaxations in pristine (n,0) CNTs, we have found that the electron and hole relaxation time constants are modified, but there is not a clear trend for the change.

The electron relaxation in all the cases upon adsorption occurs very rapidly. Typically this process completes at less than 10 fs. When n = 10, the presence of the gap state facilitates the electron relaxation by a factor of 2. When n = 13, however, the electron relaxation time does increase by a factor of 2. When n = 16 and 19, the electron relaxation times are comparable with those in the corresponding pristine CNT cases. The hole relaxations, on the other hand, are all on subpicosecond time scales. Except for n = 10 where the hole relaxation time is comparable with the pristine CNT value, all the hole relaxation times differ by a factor of 2 when they are compared with the values in pristine CNT cases. In particular, the hole relaxation time constant in both n = 13 and 19 upon adsorption is doubled, while it is reduced by half when n = 16.

Since the LUMO is the gap state in all the four cases and the initially photoexcited electron is in the CNT, when the intraband relaxation in the conduction band is complete, there is an electron transfer from the CNT to the adsorbate. As an example, Figure 5C shows such process of the photoinduced charge transfer in the (10,0) CNT−adsorbate system. It is clear that the photoexcited electron originally in the CNT eventually hops to the adsorbate, leaving a hole inside the CNT. In each case, the electron transfer occurs at the same time scales as the intraband relaxation in the conduction band, i.e., τ^es. This process takes about 10 fs or less in all the cases.

Note that in DFT calculations there is an issue about the band gap error, which is important in the studies of interband relaxation where the photoexcited electron in the conduction band recombines with the hole in the valence band. In the semiconducting CNTs, such relaxation is on time scales of 10 ps or even 100 ps,[34,57] which is at least an order of magnitude larger than the intraband relaxation aided by phonons. In the present work, since we mainly study the dynamics of the latter, we do not expect that this issue significantly changes our results. However, more accurate calculations such as the hybrid functional calculations[58] or the GW method[59,60] to correct the band gap will be applied in the future. In addition, we assume that upon photoexcitation the geometrical distortion is small so that the Huang−Rhys factors,[61] which measure the contributions of phonon modes to the reorganization energy, are negligible. We also assume that the electron−phonon interaction is weak such that the intraband relaxation dynamics can be studied within Redfield theory using the Markov approximation. Such approximations are justified by the fact that the calculated time constants for pristine CNTs are in good agreement with experiments. However, more rigorous approaches such as the nonequilibrium Green's function based technique, where those interactions are described by the non-Markovian relaxation terms in the Kadanoff−Baym equations,[62] can be applied in the future. Finally, in our calculations we have neglected excitonic effects concerning the interaction between the photoexcited electron and the hole. With all the approximations mentioned above, our results agree surprisingly well with the experiments for the pristine semiconducting (n,0) CNTs.[34,36,37] However, more advanced studies including these effects will be addressed in the future.

IV. CONCLUSIONS

We have studied semiconducting (n,0) CNTs for n = 10, 13, 16, and 19 that are functionalized by a physisorbed electron-accepting functional group, dinitromethane or $CH_2N_2O_4$. We find that the functional group can be firmly attached to the tube using a pyrene anchoring fragment. The functional group contributes additional states in the band gap of the CNT, but the pyrene fragment acts only as an anchor that enhances the binding between the dinitromethane and the CNT. In order to reduce computational intensity, the set of smaller systems, CNTs with the functional group only, has been used for further investigations. We find that an excited state of the functionalized CNT undergoes electronic dynamics coupled to thermal lattice vibrations, and electronic energy dissipates into lattice vibrations.

Furthermore, our studies of the dynamics of intraband relaxations indicate that upon initial photoexcitation an electron from the CNT ends up being transferred to the adsorbate, while a hole stays in the CNT. Electronic-state dynamics demonstrates two effects: (i) electrons and holes lose their energy into thermal vibrations, and (ii) electrons and holes migrate in space. Such migration often leads to the formation of a charge separation state. We have quantified electronic relaxation with rate constants. The photoinduced charge transfer completes in about 10 fs in all cases. For pristine CNTs, the calculated intraband relaxation time constants agree well with the experimental time scales. Our calculations predict that electron relaxation in the conduction band is faster than hole relaxation in the valence band in such CNT systems, with and without the adsorbed dinitromethane molecules. This is due to the stronger electron−phonon interaction in the conduction band than the hole−phonon interaction in the valence band.

Our results have twofold importance: (i) we demonstrate the applicability of the density matrix formulation in the Kohn−Sham DFT framework to a broader range of systems, and (ii) our results provide an important step toward developing solar energy harvesting materials.

■ AUTHOR INFORMATION

Corresponding Author

*E-mail cheng@qtp.ufl.edu; Tel 352-392-6256 (H.-P.C.).

Notes

The authors declare no competing financial interest.

■ ACKNOWLEDGMENTS

I. H. Chu and H. P. Cheng acknowledge support by the Department of Energy (DOE), Office of Basic Energy Sciences

(BES), under Contract DE-FG02-02ER45995. D. S. Kilin acknowledges support by the DOE, BES-Chemical Sciences, under Contract DE-AC02-05CH11231, Allocation Award 86185, and US National Science Foundation Award EPS0903804. The calculations are performed at NERSC and UF-HPC Center.

REFERENCES

(1) Saito, R.; Dresselhaus, G.; Dresselhaus, M. S. *Physical Properties of Carbon Nanotubes*; Imperial College Press: London, 1998.

(2) Bachilo, S. M.; Strano, M. S.; Kittrell, C.; Hauge, R. H.; Smalley, R. E.; Weisman, R. B. Structure-Assigned Optical Spectra of Single-Walled Carbon Nanotubes. *Science* **2002**, *298*, 2361−2366.

(3) Doorn, S. K.; Goupalov, S.; Satishkumar, B. C.; Shreve, A. P.; Haroz, E. H.; Bachilo, S. M.; Weisman, R. B. Raman Studies of Electron-Phonon Coupling in Single Walled Carbon Nanotubes. *Phys. Status Solidi B* **2006**, *243*, 3171−3175.

(4) Collins, P. G.; Bradley, K.; Ishigami, M.; Zettl, A. Extreme Oxygen Sensitivity of Electronic Properties of Carbon Nanotubes. *Science* **2000**, *287*, 1801−1804.

(5) Sippel-Oakley, J.; Wang, H. T.; Kang, B. S.; Wu, Z. C.; Ren, F.; Rinzler, A. G.; Pearton, S. J. Carbon Nanotube Films for Room Temperature Hydrogen Sensing. *Nanotechnology* **2005**, *16*, 2218−2221.

(6) Zhang, T.; Mubeen, S.; Myung, N. V.; Deshusses, M. A. Recent Progress in Carbon Nanotube-Based Gas Sensors. *Nanotechnology* **2008**, *19*, 332001.

(7) Cao, C.; Kemper, A. F.; Agapito, L.; Zhang, J.-W.; He, Y.; Rinzler, A.; Cheng, H.-P.; Zhang, X.-G.; Rocha, A. R.; Sanvito, S. Non-equilibrium Green's Function Study of Pd_4-Cluster-Functionalized Carbon Nanotubes as Hydrogen Sensors. *Phys. Rev. B* **2009**, *79*, 075127.

(8) Kong, J.; Franklin, N. R.; Zhou, C. W.; Chapline, M. G.; Peng, S.; Cho, K. J.; Dai, H. J. Nanotube Molecular Wires as Chemical Sensors. *Science* **2000**, *287*, 622−625.

(9) Zhao, J. J.; Buldum, A.; Han, J.; Lu, J. P. Gas Molecule Adsorption in Carbon Nanotubes and Nanotube Bundles. *Nanotechnology* **2002**, *13*, 195−200.

(10) Kymakis, E.; Amaratunga, G. A. J. Single-Wall Carbon Nanotube/Conjugated Polymer Photovoltaic Devices. *Appl. Phys. Lett.* **2002**, *80*, 112−114.

(11) Bhattacharyya, S.; Kymakis, E.; Amaratunga, G. A. J. Photovoltaic Properties of Dye Functionalized Single-Wall Carbon Nanotube/Conjugated Polymer Devices. *Chem. Mater.* **2004**, *16*, 4819−4823.

(12) Jia, Y.; Cao, A.; Bai, X.; Li, Z.; Zhang, L.; Guo, N.; Wei, J.; Wang, K.; Zhu, H.; Wu, D.; et al. Achieving High Efficiency Silicon-Carbon Nanotube Heterojunction Solar Cells by Acid Doping. *Nano Lett.* **2011**, *11*, 1901−1905.

(13) Jung, Y.; Li, X.; Rajan, N. K.; Tayor, A. D.; Reed, M. A. Record High Efficiency Single-Walled Carbon Nanotube/Silicon p-n Junction Solar Cells. *Nano Lett.* **2013**, *13*, 95−99.

(14) Chen, J.; Li, B.; Zheng, J.; Zhao, J.; Zhu, Z. Role of Carbon Nanotubes in Dye-Sensitized TiO_2-Based Solar Cells. *J. Phys. Chem. C* **2012**, *116*, 14848−14856.

(15) Yu, D.; Xue, Y.; Dai, L. Vertically Aligned Carbon Nanotube Arrays Co-doped with Phosphorus and Nitrogen as Efficient Metal-Free Electrocatalysts for Oxygen Reduction. *J. Phys. Chem. Lett.* **2012**, *3*, 2863−2870.

(16) Shi, C.; Zhang, Y.; Gu, C.; Seballos, L.; Zhang, J. Z. Manipulation and Light-Induced Agglomeration of Carbon Nanotubes through Optical Trapping of Attached Silver Nanoparticles. *Nanotechnology* **2008**, *19*, 215304.

(17) Du, M. H.; Cheng, H.-P. Manipulation of Fullerene-induced Impurity States in Carbon Peapods. *Phys. Rev. B* **2003**, *68*, 113402.

(18) Micha, D. A.; Kilin, D. S. Relaxation of Photoexcited Electrons at a Nanostructured Si(111) Surface. *J. Phys. Chem. Lett.* **2010**, *1*, 1073−1077.

(19) (a) Inerbaev, T. M.; Kilin, D. S.; Hoefelmeyer, J. Atomistic Simulation of Dissipative Charge Carrier Dynamics for Photocatalysis. *MRS Proc.* **2012**, *1390*, mrsf11-1390−i03-03. (b) Inerbaev, T.; Hoefelmeyer, J.; Kilin, D. S. Photoinduced Charge Transfer from Titania to Surface Doping Site. *J. Phys. Chem. C* **2013**, *117*, 9673−9692.

(20) Chen, J.; Schmitz, A.; Kilin, D. S. Computational Simulation of the p-n Doped Silicon Quantum Dot. *Int. J. Quantum Chem.* **2012**, *112*, 3879−3888.

(21) (a) Fernandez-Alberti, S.; Kleiman, V. D.; Tretiak, S.; Roitberg, A. E. Nonadiabatic Molecular Dynamics Simulations of the Energy Transfer between Building Blocks in a Phenylene Ethynylene Dendrimer. *J. Phys. Chem. A* **2009**, *113*, 7535−7542. (b) Fernandez-Alberti, S.; Kleiman, V. D.; Tretiak, S.; Roitberg, A. E. Unidirectional Energy Transfer in Conjugated Molecules: The Crucial Role of High-Frequency C≡C Bonds. *J Phys. Chem. Lett.* **2010**, *1*, 2699−2704. (c) Nelson, T.; Fernandez-Alberti, S.; Chernyak, V.; Roitberg, A. E.; Tretiak, S. Nonadiabatic Excited-State Molecular Dynamics Modeling of Photoinduced Dynamics in Conjugated Molecules. *J. Phys. Chem. B* **2011**, *115*, 5402−5414. (d) Nelson, T.; Fernandez-Alberti, S.; Chernyak, V.; Roitberg, A. E.; Tretiak, S. Nonadiabatic Excited-State Molecular Dynamics: Numerical Tests of Convergence and Parameters. *J. Chem. Phys.* **2012**, *136*, 054108.

(22) Runge, E.; Gross, E. K. U. Density-Functional Theory for Time-Dependent Systems. *Phys. Rev. Lett.* **1984**, *52*, 997−1000.

(23) (a) Born, M.; Oppenheimer, R. Zur Quantentheorie der Molekeln. *Ann. Phys.* **1927**, *84*, 457−484. (b) Barnett, R. N.; Landman, U.; Nitzan, A.; Rajagopal, G. Born-Oppenheimer Dynamics Using Density-Functional Theory: Equilibrium and Fragmentation of Small Sodium Clusters. *J. Chem. Phys.* **1991**, *94*, 608−616.

(24) Car, R.; Parrinello, M. Unified Approach for Molecular Dynamics and Density-Functional Theory. *Phys. Rev. Lett.* **1985**, *55*, 2471−2474.

(25) Tully, J. C. Molecular Dynamics with Electronic Transitions. *J. Chem. Phys.* **1990**, *93*, 1061−1071.

(26) Craig, C. F.; Duncan, W. R.; Prezhdo, O. V. Trajectory Surface Hopping in the Time-Dependent Kohn-Sham Approach for Electron-Nuclear Dynamics. *Phys. Rev. Lett.* **2005**, *95*, 163001.

(27) Habenicht, B. F.; Craig, C. F.; Prezhdo, O. V. Time-Domain *Ab Initio* Simulation of Electron and Hole Relaxation Dynamics in a Single-Wall Semiconducting Carbon Nanotube. *Phys. Rev. Lett.* **2006**, *96*, 187401.

(28) To the authors' knowledge there is no major difference between real-time TD-DFT [Lopata, K.; Govind, N. Modeling Fast Electron Dynamics with Real-Time Time-Dependent Density Functional Theory: Application to Small Molecules and Chromophores. *J. Chem. Theory Comput.* **2011**, *7*, 1344−1355] and the time-dependent Kohn−Sham approach. The development of electron dynamics methods was begun later than the excited-state methodology. The terminology abbreviation TDDFT was accepted by community with respect to the excited-state treatment by Casida's equations. Later developments of electron relaxation methods based on DFT experience difficulty with appropriate naming the new methodology and avoiding the abbreviation TDDFT (Casida), used earlier for excited-state energies, not for relaxation. Several attempts were used for naming of the very similar electron relaxation methods. They all try to highlight the development of the electronic state in time rather than finding energies of excitations. These abbreviations are not widely accepted yet. Preliminarily, one refers to real-time TD-DFT for propagating dynamics of excitons, while the time-dependent Kohn−Sham (TDKS) approach relates to propagating dynamics of the independent charge carriers.

(29) May, V.; Kühn, O. *Charge and Energy Transfer Dynamics in Molecular Systems*; Wiley-VCH: Berlin, 2000.

(30) (a) Redfield, A. G. On the Theory of Relaxation Processes. *IBM J. Res. Dev.* **1957**, *1*, 19−31. (b) Redfield, A. G. The Theory of Relaxation Processes. *Adv. Magn. Reson.* **1965**, *1*, 1−32.

(31) Micha, D. A.; Kilin, D. S. Atomic Modeling of Surface Photovoltage: Application to Si(1 1 1):H. *Chem. Phys. Lett.* **2008**, *461*, 266−270.
(32) Hohenberg, P.; Kohn, W. Inhomogeneous Electron Gas. *Phys. Rev.* **1964**, *136*, B864−B871.
(33) Kohn, W.; Sham, L. J. Self-Consistent Equations Including Exchange and Correlation Effects. *Phys. Rev.* **1965**, *140*, A1133−A1138.
(34) Wang, F.; Dukovic, G.; Brus, L. E.; Heinz, T. F. Time-Resolved Fluorescence of Carbon Nanotubes and Its Implication for Radiative Lifetimes. *Phys. Rev. Lett.* **2004**, *92*, 177401.
(35) Dyatlova, O. A.; Kohler, C.; Malic, E.; Gomis-Bresco, J.; Maultzsch, J.; Tsagan-Mandzhiev, A.; Watermann, T.; Knorr, A.; Woggon, U. Ultrafast Relaxation Dynamics via Acoustic Phonons in Carbon Nanotubes. *Nano Lett.* **2012**, *12*, 2249−2253.
(36) Hertel, T.; Moos, G. Electron-Phonon Interaction in Single-Wall Carbon Nanotubes: A Time-Domain Study. *Phys. Rev. Lett.* **2000**, *84*, 5002−5005.
(37) Htoon, H.; O'Connell, M. J.; Doorn, S. K.; Klimov, V. I. Single Carbon Nanotubes Probed by Photoluminescence Excitation Spectroscopy: The Role of Phonon-Assisted Transitions. *Phys. Rev. Lett.* **2005**, *94*, 127403.
(38) Graham, M. W.; Chmeliov, J.; Ma, Y.-Z.; Shinohara, H.; Green, A. A.; Hersam, M. C.; Valkunas, L.; Fleming, G. R. Exciton Dynamics in Semiconducting Carbon Nanotubes. *J. Phys. Chem. B* **2011**, *115*, 5201−5211.
(39) Guldi, D. M.; Rahman, G. M. A.; Sgobba, V.; Kotov, N. A.; Bonifazi, D.; Prato, M. CNT-CdTe Versatile Donor-Acceptor Nanohybrids. *J. Am. Chem. Soc.* **2006**, *128*, 2315−2323.
(40) Hu, L.; Zhao, Y.-L.; Ryu, K.; Zhou, C.; Stoddart, J. F.; Grüner, G. Light-Induced Charge Transfer in Pyrene/CdSe-SWNT Hybrids. *Adv. Mater.* **2008**, *20*, 939−946.
(41) XCrysden: http://www.xcrysden.org.
(42) Quantum Espresso Package: http://www.pwscf.org.
(43) Rappe, A. M.; Rabe, K. M.; Kaxiras, E.; Joannopoulos, J. D. Optimized pseudopotentials. *Phys. Rev. B* **1990**, *41*, 1227−1230.
(44) Ceperley, D. M.; Alder, B. J. Ground State of the Electron Gas by a Stochastic Method. *Phys. Rev. Lett.* **1980**, *45*, 566−569.
(45) Perdew, J. P.; Burke, K.; Ernzerhof, M. Generalized Gradient Approximation Made Simple. *Phys. Rev. Lett.* **1996**, *77*, 3865−3868.
(46) Grimme, S. Semiempirical GGA-Type Density Functional Constructed with a Long-Range Dispersion Correction. *J. Comput. Chem.* **2006**, *27*, 1787−1799.
(47) Dion, M.; Rydberg, H.; Schroder, E.; Langreth, D. C.; Lundqvist, B. I. Van der Waals Density Functional for General Geometries. *Phys. Rev. Lett.* **2004**, *92*, 246401.
(48) Roman-Perez, G.; Soler, J. M. Efficient Implementation of A van der Waals Density Functional: Application to Double-Wall Carbon Nanotubes. *Phys. Rev. Lett.* **2009**, *103*, 096102.
(49) Woods, L. M.; Badescu, S. C.; Reinecke, T. L. Adsorption of Simple Benzene Derivatives on Carbon Nanotubes. *Phys. Rev. B* **2007**, *75*, 155415.
(50) Kresse, G.; Hafner, J. *Ab Initio* Molecular Dynamics for Liquid Metals. *Phys. Rev. B* **1993**, *47*, 558−561.
(51) Kresse, G.; Furthmuller, J. Efficient Iterative Schemes for *Ab Initio* Total-Energy Calculations Using A Plane-Wave Basis Set. *Phys. Rev. B* **1996**, *54*, 11169−11186.
(52) Blochl, P. E. Projector Augmented-Wave Method. *Phys. Rev. B* **1994**, *50*, 17953−17979.
(53) Klimes, J.; Bowler, D. R.; Michaelides, A. Van der Waals Density Functionals Applied to Solids. *Phys. Rev. B* **2011**, *83*, 195131.
(54) Habenicht, B. F.; Kamisaka, H.; Yamashita, K.; Prezhdo, O. V. *Ab Initio* Study of Vibrational Dephasing of Electronic Excitations in Semiconducting Carbon Nanotubes. *Nano Lett.* **2007**, *7*, 3260−3265.
(55) Shreve, A. P.; Haroz, E. H.; Bachilo, S. M.; Weisman, R. B.; Tretiak, S.; Kilina, S.; Doorn, S. K. Determination of Exciton-Phonon Coupling Elements in Single-Walled Carbon Nanotubes by Raman Overtone Analysis. *Phys. Rev. Lett.* **2007**, *98*, 037405.
(56) Kilin, D. S.; Tsemekhman, K.; Prezhdo, O. V.; Zenkevich, E. I.; Borczyskowski, C. v. *Ab Initio* Study of Exciton Transfer Dynamics from A Core-Shell Semiconductor Quantum Dot to a Porphyrin-Sensitizer. *J. Photochem. Photobiol. A: Chem.* **2007**, *190*, 342−351.
(57) Ostojic, G. N.; Zaric, S.; Kono, J.; Strano, M. S.; Moore, V. C.; Hauge, R. H.; Smalley, R. E. Interband Recombination Dynamics in Resonantly Excited Single-Walled Carbon Nanotubes. *Phys. Rev. Lett.* **2004**, *92*, 117402.
(58) Heyd, J.; Scuseria, G. E.; Ernzerhof, M. Hybrid Functionals Based on A Screened Coulomb Potential. *J. Chem. Phys.* **2003**, *118*, 8207−8215.
(59) Hedin, L. New Method for Calculating the One-Particle Green's Function with Application to the Electron-Gas Problem. *Phys. Rev.* **1965**, *139*, A796−A823.
(60) Hybertsen, M. S.; Louie, S. G. Electron Correlation in Semiconductors and Insulators: Band Gaps and Quasiparticle Energies. *Phys. Rev. B* **1986**, *34*, 5390−5413.
(61) Huang, K.; Rhys, A. Theory of Light Absorption and Non-Radiative Transitions in F-Centres. *Proc. R. Soc.* **1950**, *204*, 406−423.
(62) Kolesov, G.; Dahnovsky, Y. Correlated Electron Dynamics in Quantum-Dot Sensitized Solar Cell: Kadanoff-Baym Versus Markovian Approach. *Phys. Rev. B* **2012**, *85*, 241309(R).